


Cite this: *RSC Adv.*, 2019, 9, 39242

# Preparation of a SnO<sub>2</sub>–Sb electrode on a novel TiO<sub>2</sub> network structure with long service lifetime for degradation of dye wastewater

Li Xu,<sup>ab</sup> Ye Wang<sup>ab</sup> and Wen Zhang \*<sup>ab</sup>

Developing effective electrodes with long service lifetime for electrochemical degradation of dyes is of paramount importance for their practical industrial applications. We constructed a novel SnO<sub>2</sub>–Sb electrode (Ti/TiO<sub>2</sub>–NW/SnO<sub>2</sub>–Sb electrode) based on a uniform TiO<sub>2</sub> network structure decorated Ti plate (Ti/TiO<sub>2</sub>–NW) for a long-term electrocatalytic performance. The SnO<sub>2</sub>–Sb coating layer on this electrode was grown on the Ti/TiO<sub>2</sub>–NW by pulse electrodeposition. The introduction of the three-dimensional TiO<sub>2</sub>–NW enhances the bonding strength between the Ti substrate and the SnO<sub>2</sub>–Sb surface coating. An accelerated life test shows that the service life of Ti/TiO<sub>2</sub>–NW/SnO<sub>2</sub>–Sb electrode is 11.15 times longer than that of the traditional Ti/SnO<sub>2</sub>–Sb electrode. The physicochemical properties of the electrodes were characterized through SEM, EDS, XRD and HRTEM. In addition, through LSV, EIS, CV and voltammetric charge analysis, it is found that compared with the traditional electrode, the Ti/TiO<sub>2</sub>–NW/SnO<sub>2</sub>–Sb electrode possesses a higher oxygen evolution potential, a lower charge transfer resistance and a larger electrochemical active surface area. Besides, this novel electrode also exhibits an outstanding electrocatalytic oxidation ability for degradation of acid red 73 in simulated sewage. After a 5 hours' test, the removal efficiency of acid red 73 and the COD reached 98.6% and 71.8%, respectively, which were superior to those of Ti/SnO<sub>2</sub>–Sb electrode (89.1% and 58.8%). This study highlights the excellent stability of the Ti/TiO<sub>2</sub>–NW/SnO<sub>2</sub>–Sb electrode and provides an energy-efficient strategy for dye degradation.

Received 24th July 2019  
Accepted 21st November 2019

DOI: 10.1039/c9ra05713g

rsc.li/rsc-advances

## 1. Introduction

The shortage of water resources is a problem that human beings need to solve urgently. As one of the main sources of water pollution (about 280 000 tons of textile dyes are discharged annually in the form of wastewater<sup>1</sup>), dye wastewater has been extensively studied due to its difficulty to degrade and the fact that it contains toxic substances. At present, the common treatment methods of dye wastewater mainly include electrochemistry, biodegradation,<sup>2</sup> membrane separation,<sup>3</sup> flocculation and sedimentation.<sup>4</sup> Among them, electrocatalytic oxidation technology has attracted increasing attention because of its strong catalytic ability and good environmental compatibility.<sup>5</sup> The efficiency of this technology is greatly affected by the electrode materials.<sup>6,7</sup> Various kinds of electrodes, including IrO<sub>2</sub>,<sup>8</sup> RuO<sub>2</sub>,<sup>9</sup> boron-doped diamond (BDD),<sup>10</sup> Pt,<sup>11</sup> PbO<sub>2</sub> (ref. 12) and SnO<sub>2</sub>, have been studied. Compared with other electrodes, SnO<sub>2</sub> electrode has been well known for its high oxygen evolution potential, low cost and efficient electro-generation of

•OH.<sup>13,14</sup> However, the high charge transfer resistance and low physicochemical stability of SnO<sub>2</sub> decreases its application value. Lots of studies have shown that doping Sb into SnO<sub>2</sub> can significantly improve its charge transfer ability and produce more •OH, which is conducive to the electrocatalytic reaction.

Although the characteristics of Sb-doped SnO<sub>2</sub> have been improved to some extent, the short service life of the SnO<sub>2</sub>–Sb electrode still restrains its practical application. A large number of efforts are being spent to solve this problem. Some researchers have tried to dope elements into the SnO<sub>2</sub>–Sb coating, such as rare earth elements (Ce, Eu, Gd, *etc.*<sup>15,16</sup>) and non-rare earth metal elements (Fe, Bi, Pd, *etc.*<sup>17–19</sup>). Doping these elements can change the structure of the surface coating, thus enhancing the stability of the coating to some extent. Similarly, the introduction of the novel surface morphology (nanorods, nanoflowers, nanobelts, *etc.*<sup>20,21</sup>) can also change the surface coating to improve the electrodes' electrocatalytic activity. However, the service life of electrodes decorated by these nanostructured surface coating has not been increased obviously. As we know, the factors that affect the stability of the electrode are very complicated and have not been studied thoroughly. But it is generally believed that the poor bonding force between the substrate and surface coating is the main factor causing the deactivation of electrodes.<sup>22,23</sup>

<sup>a</sup>School of Chemical Engineering and Technology, Tianjin University, Tianjin 300350, People's Republic of China. E-mail: zhang\_wen@tju.edu.cn

<sup>b</sup>Tianjin Key Laboratory of Membrane Science and Desalination Technology, Tianjin 300350, People's Republic of China



Therefore, the study of improving the bonding force between the substrate and surface coating has attracted considerable attention. On one hand, some researchers employed different preparation methods for electrode surface coating to improve the bonding force. Chen *et al.*<sup>24</sup> founded that the service life of Ti/SnO<sub>2</sub>-Sb electrode prepared by electrodeposition is 6.25 times as much as that prepared by thermal decomposition. On the other hand, adding an interlayer is also considered as an effective way to improve the bonding force. Xu *et al.*<sup>25</sup> deposited a Cu nanorods interlayer through the anodic aluminum oxide (AAO) template before making the SnO<sub>2</sub>-Sb layers. Compared with the Ti/SnO<sub>2</sub>-Sb electrode, the service lifetime of the Ti/Cu-NRs/SnO<sub>2</sub>-Sb electrode is increased by 1.63 times. As a novel intermediate layer, the TiO<sub>2</sub> nanotube structure can be directly prepared on the Ti plate by anodization.<sup>26</sup> Then it can be used as an excellent tubular template for microstructures, in which SnO<sub>2</sub>-Sb is implanted to obtain stacked microstructures and increase the specific surface area of the electrodes.<sup>27</sup> Moreover, the TiO<sub>2</sub> nanotube structure does not include other elements except Ti and O, so it has been extensively studied. Li *et al.*<sup>28</sup> introduced the TiO<sub>2</sub> nanotube structure into the SnO<sub>2</sub> electrode, prolonging the electrode service life from 22 h to 45 h and improving the electrochemical performance of the electrode.

The main purpose of the current research is to enhance the service life of the SnO<sub>2</sub>-Sb electrode. To achieve it, a novel TiO<sub>2</sub>-NW was introduced onto the Ti substrate by hydrothermal method, and then the SnO<sub>2</sub>-Sb surface coating was fabricated *via* pulsed electrodeposition. The morphologies and element compositions of the electrode were characterized by SEM and EDS. The crystal structure was further obtained by XRD and HRTEM. Then, the electrochemical properties were studied through LSV, EIS, CV and voltammetric charge analysis. Accelerated service life test was performed to evaluate the stability of the electrodes and the deactivation mechanism was further studied by SEM, EDS and EIS. Finally, the electrocatalytic performance was studied through degrading acid red 73.

## 2. Experimental

### 2.1. Preparation of TiO<sub>2</sub> network

The TiO<sub>2</sub> network structure (TiO<sub>2</sub>-NW) was prepared by a typical hydrothermal process mentioned in ref. 29. Prior to hydrothermal synthesis, the Ti sheets (20 mm × 20 mm × 0.5 mm) were polished using 240-grit sandpaper, and degreased in 5 wt% NaOH at 90 °C for 1 h. Then, the Ti plates were etched in 10 wt% oxalic acid at 99 °C for 2 h, washed with deionized water and dried. For the hydrothermal synthesis, 4 mL of ethanol was poured into 32 mL of 0.5 mol L<sup>-1</sup> NaOH solution and stirred for 10 minutes to form a uniform precursor solution. Then a pretreated Ti plate was transferred into a 50 mL Teflon-lined stainless-steel autoclave with the precursor solution. The hydrothermal reaction was performed at 220 °C for 16 h, and cooled to ambient temperature naturally. Then, the Ti plate was rinsed with deionized water, and immersed in 50 mL of 0.1 mol L<sup>-1</sup> HCl for 6 h to replace Na<sup>+</sup> on the plate with H<sup>+</sup>. Finally, the Ti plate was washed with distilled water and

annealed at 500 °C in oxygen ambient for 2 h (with a heating rate of 4 °C min<sup>-1</sup>) to obtain the TiO<sub>2</sub> network structure.

### 2.2. Preparation of Ti/TiO<sub>2</sub>-NW/SnO<sub>2</sub>-Sb electrode

Before depositing, the TiO<sub>2</sub> network structure was reduced in 5 wt% Na<sub>2</sub>SO<sub>4</sub> solution by an electrochemical cathodic reduction process (two-electrode system; nickel plate was used as the counter electrode; the current density was 20 mA cm<sup>-2</sup>; reduction time 20 min) to improve conductivity.<sup>30</sup> The SnO<sub>2</sub>-Sb surface coating was prepared by pulse electrodeposition for 90 min and the details of current density parameter were shown in ref. 20. The electrolyte contained 0.047 M tartaric acid (C<sub>4</sub>H<sub>6</sub>O<sub>6</sub>), 0.25 M sodium pyrophosphate tetrabasic decahydrate (Na<sub>4</sub>P<sub>2</sub>O<sub>7</sub>·10H<sub>2</sub>O), 0.13 M two hydrated stannous chloride (SnCl<sub>2</sub>·2H<sub>2</sub>O), 0.02 M trichloroantimony (SbCl<sub>3</sub>) and 0.8 g L<sup>-1</sup> gelatin.<sup>25</sup> Finally, the electrode was annealed at 500 °C for 2 h (with a heating rate of 1 °C min<sup>-1</sup>).

In contrast, the pretreated Ti plate went directly through the same pulse electrodeposition procedures without the hydrothermal process to fabricate a traditional Ti/SnO<sub>2</sub>-Sb electrode.

### 2.3. Characterization of electrodes

A field emission scanning electron microscope (S-4800, Japan) equipped with energy-dispersive spectrometer (EDS) was used to examine the surface morphology and element composition of electrodes. X-ray diffraction (XRD) with Cu-Kα ray (λ = 0.15406 nm; 40 kV, 40 mA) was applied to identify the crystal structure of the electrodes in a 2θ range from 20° to 80°. A transmission electron microscopy (JEM-2100F) was used to further determine the crystal structure.

Electrochemical measurements were carried out *via* an electrochemical workstation (PARSTAT 2273, PARC, USA) in a conventional three-electrode cell. The fabricated electrodes were employed as working electrode, while a Pt sheet (40 mm × 40 mm) and an Ag/AgCl/0.1 M KCl served as the counter electrode and reference electrode, respectively. 0.5 M H<sub>2</sub>SO<sub>4</sub> was used as electrolyte. The linear sweep voltammetry (LSV) was carried out between 1.0 V and 2.5 V. The electrochemical impedance spectroscopy (EIS) was performed in the range of 10<sup>5</sup> to 10<sup>-2</sup> Hz. The cyclic voltammetry (CV) was conducted between 0.3 V and 1.5 V. Besides, to investigate the reaction process of the electrode, 100 mg L<sup>-1</sup> AR 73 solution was added in the CV test.

An accelerated life test was applied to assess the electrode stability, which was conducted in 0.5 M H<sub>2</sub>SO<sub>4</sub> with a current density of 1 A cm<sup>-2</sup> and 250 mA cm<sup>-2</sup>. The anode potential was measured as a function of time, considering that the electrode was deactivated when this potential increased 5 V from its initial value.<sup>31</sup>

### 2.4. Electrocatalytic degradation process

Acid red 73 (AR 73) is selected as simulated wastewater and its details are shown in ref. 25. The electrocatalytic performance of the electrodes was tested by degrading AR 73 during which a three-electrode degradation system was used. The fabricated electrode was used as the anode and two ordinary Ti plates with



the same area were used as the cathode. In the electrolysis test, 110 mL of 100 mg L<sup>-1</sup> AR 73 solution was poured into the cell with 0.1 M Na<sub>2</sub>SO<sub>4</sub> as the supporting electrolyte. The current density was fixed to 20 mA cm<sup>-2</sup> by a DC potentiostat. The AR 73 concentration during the electrocatalytic process was monitored by UV-visible spectrophotometer. The chemical oxygen demand (COD) was measured by COD reactor and spectrophotometer (DR1010 COD, HACH, USA).

### 3. Results and discussion

#### 3.1. Morphology and crystal structure

Compared with the Ti substrate (Fig. 1a), it is observed from Fig. 1b that the uniform TiO<sub>2</sub>-NW has been successfully formed through the hydrothermal process. The TiO<sub>2</sub>-NW consists of meshes with an average diameter of about 5 μm, filled with filamentous fibers with an average width of less than 100 nm. Fig. 1c and d show the morphology of Ti/SnO<sub>2</sub>-Sb and Ti/TiO<sub>2</sub>-NW/SnO<sub>2</sub>-Sb electrodes, respectively. It is seen that the surface of Ti/SnO<sub>2</sub>-Sb electrode is distributed with spherical particles of different sizes (the average size is about 15 μm) and some particles are agglomerated. As a comparison, Ti/TiO<sub>2</sub>-NW/SnO<sub>2</sub>-Sb electrode has a smaller particle size (the average size is about 6 μm) and the particles distribute more closely. It can be inferred that the large specific surface area of TiO<sub>2</sub>-NW provides more growth sites than that of Ti substrate, which increases the rate of nucleation speed and decreases the size of nucleation. The insets of Fig. 1c and d show the magnification image of the

electrodes. We can see the surface of the particles on the Ti/SnO<sub>2</sub>-Sb electrode is smoother while the Ti/TiO<sub>2</sub>-NW/SnO<sub>2</sub>-Sb electrode is filled with smaller particles, which lead the Ti/TiO<sub>2</sub>-NW/SnO<sub>2</sub>-Sb electrode to have a larger specific surface area. The coating thickness of electrodes is further compared in Fig. 1e and f. It can be seen that the coating thickness of Ti/SnO<sub>2</sub>-Sb electrode (111.0 μm) is larger than that of Ti/TiO<sub>2</sub>-NW/SnO<sub>2</sub>-Sb electrode (95.1 μm), which may be due to the dense distribution of Ti/TiO<sub>2</sub>-NW/SnO<sub>2</sub>-Sb electrode's particles.

EDS was employed to determine the elemental composition of the electrode catalytic coating. According to Table 1, the Sn, Sb and O elements are detected on two kinds of electrodes, indicating that the Sn, Sb elements were successfully deposited on the surface of the electrodes. Meanwhile, Ti element is not detected on both electrodes, which indicates that the SnO<sub>2</sub>-Sb active coating prepared by pulse electrodeposition provides good coverage of the Ti substrate.

To further investigate the microstructure of the electrodes, XRD measurement was performed to analyze the crystal structure. Fig. 2a presents XRD patterns of TiO<sub>2</sub>-NW, and TiO<sub>2</sub> with anatase phase corresponding to (110) reflection can be found. In Fig. 2b, the diffraction peaks' positions of the two kinds of electrodes agree well with the reflections of rutile SnO<sub>2</sub> (PDF#41-1445). No peaks of antimony oxides were found because Sb entered into the SnO<sub>2</sub> lattice to form a solid solution.<sup>32</sup> The results of HRTEM showed that the fringe interval of 0.26 nm and 0.14 nm was in agreement with the interplanar spacing of (101) and (301) crystal planes of SnO<sub>2</sub>. The crystal phase of Sb was not found, which further indicated that the solid solution of SnO<sub>2</sub>-SbO<sub>x</sub> formed. In addition, the diffraction peak intensity of the Ti/TiO<sub>2</sub>-NW/SnO<sub>2</sub>-Sb electrode is obviously higher than that of the Ti/SnO<sub>2</sub>-Sb electrode, especially the (110), (101), and (211) crystal planes, indicating the TiO<sub>2</sub>-NW can enhance the crystallinity of the electrodes. The lattice parameters of electrodes were calculated by Bragg's formula.<sup>33</sup> By comparison, the lattice parameters of Ti/TiO<sub>2</sub>-NW/SnO<sub>2</sub>-Sb electrode (*a* = *b* = 0.4727 nm, *c* = 0.3184 nm) and Ti/SnO<sub>2</sub>-Sb electrode (*a* = *b* = 0.4735 nm, *c* = 0.3186 nm) are smaller than that of standard lattice parameter of SnO<sub>2</sub> (*a* = *b* = 0.4738 nm, *c* = 0.3187 nm). This is because Sb<sup>5+</sup> has been doped in the SnO<sub>2</sub> unit cell and the radius of Sb<sup>5+</sup> (0.74 Å) is smaller than that of Sn<sup>4+</sup> (0.83 Å).<sup>32</sup> Scherrer formula was used to calculate the average crystal size of the electrodes. The results demonstrate that the crystal size of the Ti/TiO<sub>2</sub>-NW/SnO<sub>2</sub>-Sb electrode (58.91 nm) is smaller than that of Ti/SnO<sub>2</sub>-Sb electrode (87.42 nm),

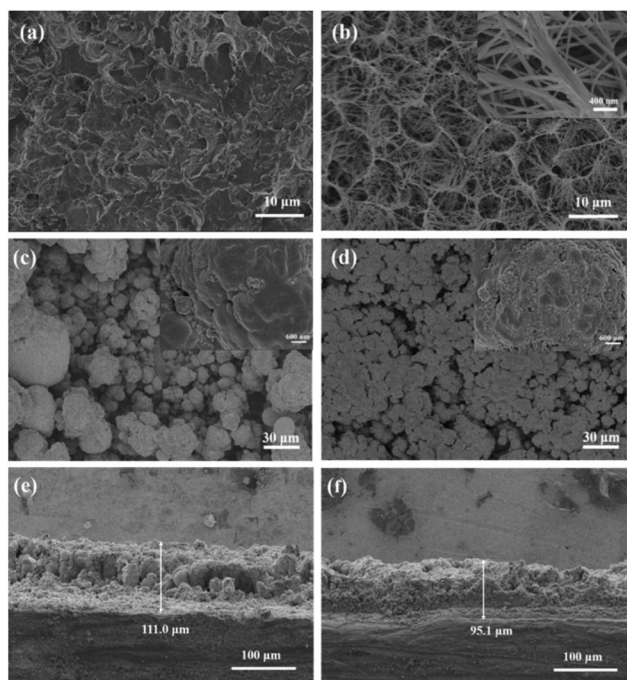


Fig. 1 (a) SEM image of Ti substrate; (b) SEM image of TiO<sub>2</sub> network; (c) SEM image of Ti/SnO<sub>2</sub>-Sb; (d) SEM image of Ti/TiO<sub>2</sub>-NW/SnO<sub>2</sub>-Sb; (e) the cross section of Ti/SnO<sub>2</sub>-Sb; (f) the cross section of Ti/TiO<sub>2</sub>-NW/SnO<sub>2</sub>-Sb. The insets of (b), (c) and (d) show the magnification view of the electrodes.

Table 1 The content of elements in electrodes

Electrodes	O (at%)	Sb (at%)	Sn (at%)	Ti (at%)
Ti/SnO <sub>2</sub> -Sb	49.1	6.2	44.7	—
Ti/TiO <sub>2</sub> -NW/SnO <sub>2</sub> -Sb	47.5	9.4	43.1	—
Ti/SnO <sub>2</sub> -Sb-A <sup>a</sup>	51.9	1.3	11.0	35.8
Ti/TiO <sub>2</sub> -NW/SnO <sub>2</sub> -Sb-A <sup>a</sup>	56.8	7.3	35.9	—

<sup>a</sup> A represents the electrode after accelerated life testing.





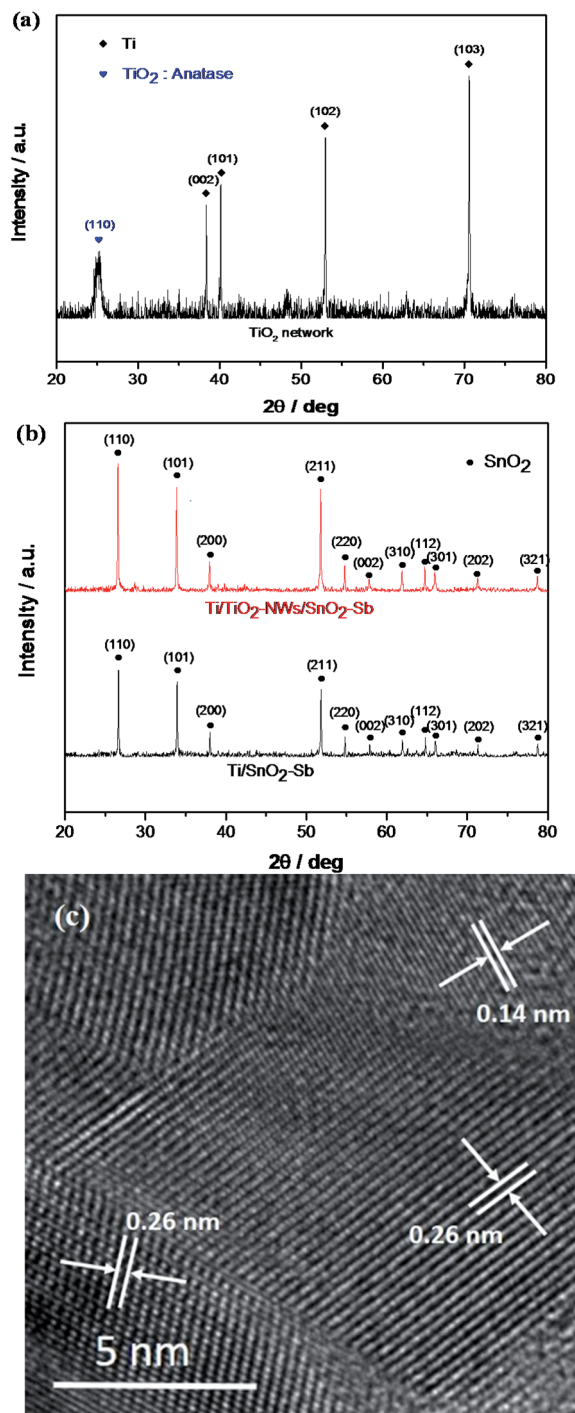


Fig. 2 (a) XRD pattern of  $\text{TiO}_2$  network; (b) XRD patterns of  $\text{Ti/SnO}_2\text{-Sb}$  and  $\text{Ti/TiO}_2\text{-NW/SnO}_2\text{-Sb}$ 's coatings; (c) HRTEM image of  $\text{Ti/TiO}_2\text{-NW/SnO}_2\text{-Sb}$  electrode.

indicating that the  $\text{Ti/TiO}_2\text{-NW/SnO}_2\text{-Sb}$  electrode has a larger specific surface area.

### 3.2. Electrochemical test

The oxygen evolution potential (OEP) of electrodes was evaluated by LSV measurement. A high OEP means a low side reaction of oxygen formation and a high current efficiency, which

would be beneficial to promote the electro-catalytic oxidation efficiency of organic pollutants.<sup>34</sup> As shown in Fig. 3, the OEP of the  $\text{Ti/TiO}_2\text{-NW/SnO}_2\text{-Sb}$  electrode is 2.28 V, which is 0.08 V higher than that of  $\text{Ti/SnO}_2\text{-Sb}$  electrode (2.20 V). This situation can be explained by the fact that  $\text{Ti/TiO}_2\text{-NW/SnO}_2\text{-Sb}$  electrode has a denser surface coating and a better crystallinity (as proved in the SEM and XRD analysis), which leads to the reduction of the lattice defects and oxygen vacancy concentration, thus further resulting the OEP to rise.<sup>35</sup> Meanwhile, the current response of  $\text{Ti/TiO}_2\text{-NW/SnO}_2\text{-Sb}$  electrode is higher, indicating the charge transfer resistance of the electrode is reduced and more  $\cdot\text{OH}$  could be produced, which will be helpful to degrade organic matter in the dye wastewater.<sup>25</sup>

EIS was used to measure the charge transfer resistance of electrodes. As displayed in Fig. 4, the points represent the experimental value and the curves represent the fitted value obtained by the Zsimpwin software. The equivalent circuit that best matched the experimental data is  $R_s(R_{ct}CPE)$ , where  $R_s$ ,  $R_{ct}$  and CPE are electrolyte resistance, charge transfer resistance and constant phase element, respectively. According to the simulation results (Table 2),  $R_{ct}$  of the  $\text{Ti/TiO}_2\text{-NW/SnO}_2\text{-Sb}$  electrode is  $25.39\ \Omega$ , which is only 28.9% of  $\text{Ti/SnO}_2\text{-Sb}$  electrode ( $87.73\ \Omega$ ). The reason could be explained as the  $\text{TiO}_2\text{-NW}$  provides a channel for the transfer of electrons. Moreover, prior to electrodepositing the surface coating, the  $\text{TiO}_2\text{-NW}$  is hydrogenated<sup>30</sup> so that the conductivity of the electrode is enhanced.

The CV test was applied to evaluate the electrochemical performance of the electrodes. As shown in Fig. 5, no other peaks appear except the one corresponding to the oxygen evolution reaction, indicating that direct electron transfer does not occur between the electrodes and the pollutant during the electrochemical oxidation process.<sup>36</sup> In addition, the area surrounded by the CV curves of the electrodes shows that the capacitance of  $\text{Ti/TiO}_2\text{-NW/SnO}_2\text{-Sb}$  electrode is obviously larger than that of the  $\text{Ti/SnO}_2\text{-Sb}$  electrode's, which is consistent with the results of EIS test (Table 2). This is because the

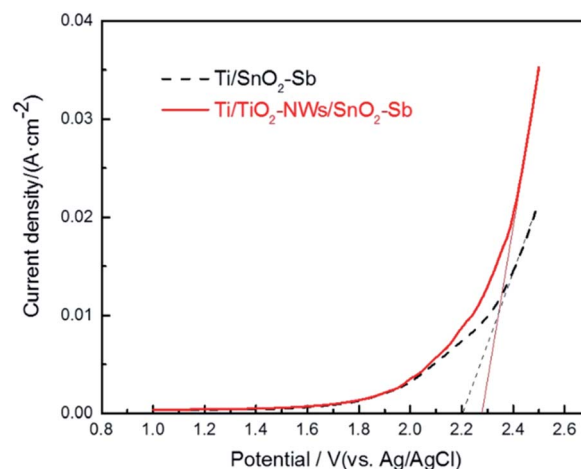


Fig. 3 Linear sweep voltammetric curves of  $\text{Ti/SnO}_2\text{-Sb}$  and  $\text{Ti/TiO}_2\text{-NW/SnO}_2\text{-Sb}$  electrodes in  $0.5\ \text{mol L}^{-1}\ \text{H}_2\text{SO}_4$  solution.



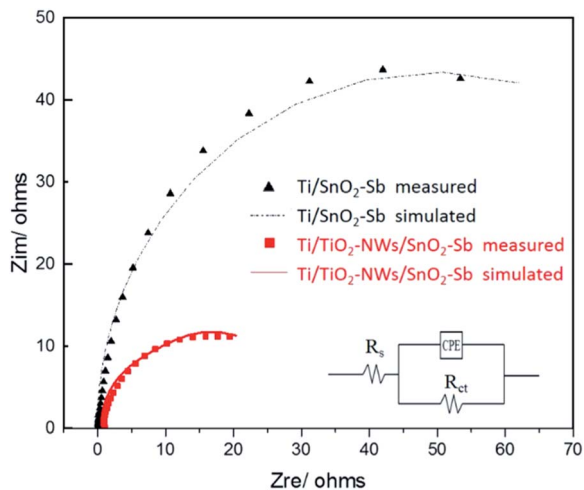


Fig. 4 Electrochemical impedance spectroscopies of Ti/SnO<sub>2</sub>-Sb and Ti/TiO<sub>2</sub>-NW/SnO<sub>2</sub>-Sb electrodes in 0.5 mol L<sup>-1</sup> H<sub>2</sub>SO<sub>4</sub> solution.

Table 2 EIS fitting analysis results of different electrodes

Electrodes	$R_s$ /ohm	$R_{ct}$ /ohm	CPE/F
Ti/SnO <sub>2</sub> -Sb	0.22	87.73	0.009
Ti/TiO <sub>2</sub> -NW/SnO <sub>2</sub> -Sb	0.99	25.39	0.027

particles of the catalytic layer on the Ti/TiO<sub>2</sub>-NW/SnO<sub>2</sub>-Sb electrode have a smaller size.<sup>37</sup>

Voltammetric charge ( $q^*$ ) was calculated to further compare the active surface area between the electrodes and it has been studied that  $q^*$  decreases as the scan rate ( $\nu$ ) increases.<sup>38,39</sup> It is worth noting that total voltammetric charge ( $q_{total}^*$ ) includes inner voltammetric charge ( $q_{in}^*$ ) and outer voltammetric charge ( $q_{out}^*$ ). When the  $\nu$  is close to  $\infty$ , the electrolyte has no

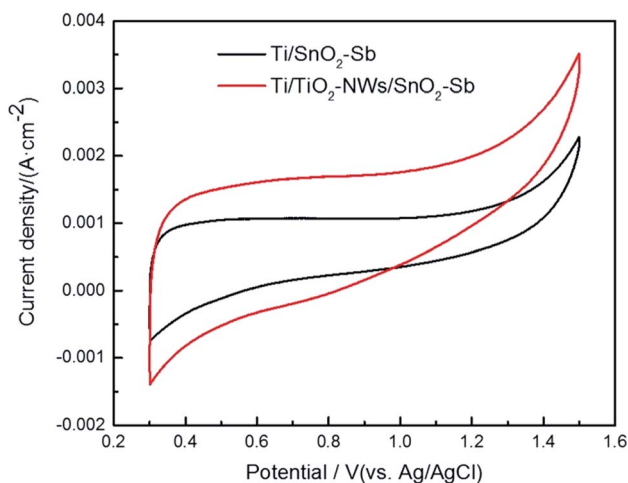


Fig. 5 Cyclic voltammograms of Ti/SnO<sub>2</sub>-Sb and Ti/TiO<sub>2</sub>-NW/SnO<sub>2</sub>-Sb electrodes in 100 mg L<sup>-1</sup> AR 73 and 0.5 mol L<sup>-1</sup> H<sub>2</sub>SO<sub>4</sub> solution at a scan rate of 50 mV s<sup>-1</sup>.

time to enter the inside of the electrode, so only the  $q_{out}^*$  participates in the reaction. The  $q_{out}^*$  is shown in Fig. 6a as the intercept of the straight lines, which can be calculated by

$$q^* = q_{out}^* + k_1 \nu^{-\frac{1}{2}} \quad (1)$$

where the  $k_1$  is the slope of the linear fitting. When the  $\nu$  is close to 0, the electrolyte has sufficient time to penetrate the catalytic layer into the electrode, and thus the  $q_{total}^*$  of the electrode participates in the reaction. Similarly, the reciprocal of  $q_{total}^*$  is shown in Fig. 6b as the intercept of the straight lines, which can be obtained according to

$$(q^*)^{-1} = (q_{total}^*)^{-1} + k_2 \nu^{\frac{1}{2}} \quad (2)$$

where the  $k_2$  is the slope of the linear fitting. And the  $q_{in}^*$  is determined by

$$q_{in}^* = q_{total}^* - q_{out}^* \quad (3)$$

The electrochemical porosity ( $r$ ) was defined as the ratio of the inner and the total charge ( $q_{in}^*/q_{total}^*$ ), which reflects the

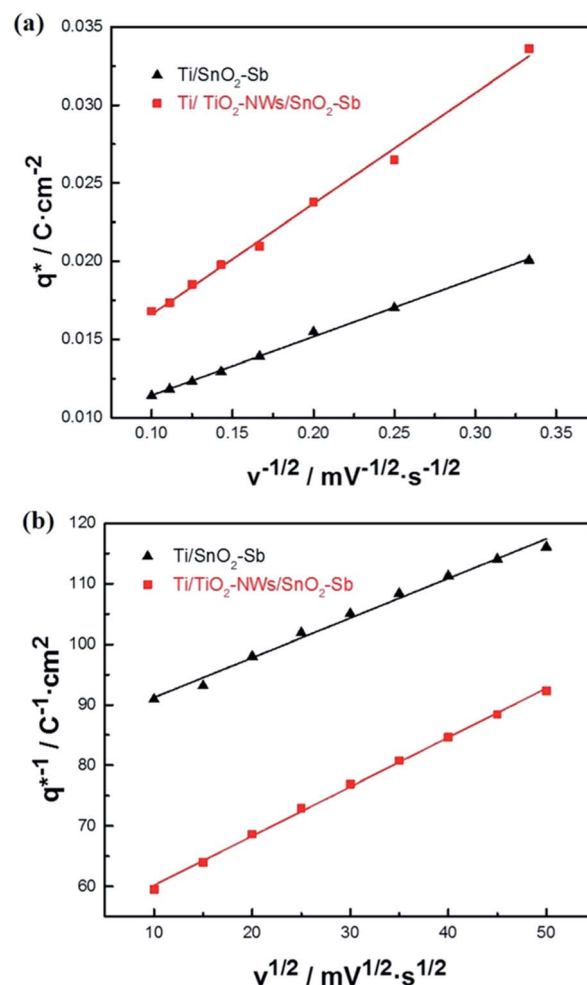


Fig. 6 (a) Voltammetric charge ( $q^*$ ) versus the reciprocal square root of the voltammetric scan rate ( $\nu^{-1/2}$ ) for different electrodes; (b) reciprocal voltammetric charge ( $q^*$ )<sup>-1</sup> versus the square root of the voltammetric scan rate ( $\nu^{1/2}$ ) for different electrodes.



microstructure of the electrode catalytic layer from another aspect. As displayed in Table 3, it can be found that the  $q_{\text{total}}^*$ ,  $q_{\text{out}}^*$  and  $q_{\text{in}}^*$  of the Ti/TiO<sub>2</sub>-NW/SnO<sub>2</sub>-Sb electrode are 1.63, 1.23, and 2.37 times of the Ti/SnO<sub>2</sub>-Sb electrode's respectively due to the introduction of TiO<sub>2</sub>-NW. Furthermore, as the amount of  $q_{\text{in}}^*$  increases significantly, the  $r$  increases by 31.3%. These results further confirmed that the active surface area of the Ti/TiO<sub>2</sub>-NW/SnO<sub>2</sub>-Sb electrode is larger than that of the Ti/SnO<sub>2</sub>-Sb electrode.

### 3.3. Electrode stability

The service life of the electrode is an important factor affecting the actual industrial application. However, it is relatively too long to measure, due to the application at low current density in practice. Hine *et al.*<sup>40</sup> proved that the service life of the electrode decreased sharply with the increase of current density. Therefore, the current density of 1 A cm<sup>-2</sup> is selected to test the electrode's accelerated life. As shown in Fig. 7a, the accelerated service life of the Ti/TiO<sub>2</sub>-NW/SnO<sub>2</sub>-Sb electrode is 111.5 min, which is 11.15 times longer than that of Ti/SnO<sub>2</sub>-Sb electrode (10 min). Meanwhile, it was clearly seen that the surface coating of the Ti/SnO<sub>2</sub>-Sb electrode detached continuously during the test, causing the electrolyte to be turbid, while the electrolyte for detecting the Ti/TiO<sub>2</sub>-NW/SnO<sub>2</sub>-Sb electrode was still clarified. In addition, the accelerated life of Ti/TiO<sub>2</sub>-NW/SnO<sub>2</sub>-Sb electrode at the current density of 250 mA cm<sup>-2</sup> was also measured (Fig. 7b). Table 4 shows the accelerated service life of the titanium-based SnO<sub>2</sub>-Sb electrodes studied in other literatures. In order to make the comparison results more intuitive, we have converted the current density of the accelerated life test to 100 mA cm<sup>-2</sup> according to the formula (4).<sup>20</sup>

$$\tau_1 = \left( \frac{i_2}{i_1} \right)^2 \tau_2 \quad (4)$$

where  $i_1$  is the actual current density,  $\tau_1$  is the actual service life,  $i_2$  is the accelerated current density and  $\tau_2$  is the accelerated service life. After comparison, it can be seen that the stability of Ti/TiO<sub>2</sub>-NW/SnO<sub>2</sub>-Sb electrode is at a higher level.

The deactivation mechanism of electrodes after accelerated life test (1 A cm<sup>-2</sup>) was further analysed by SEM and EDS. As is indicated in Fig. 8a and Table 1, most of the spherical particles on Ti/SnO<sub>2</sub>-Sb electrode have fallen off compared to Fig. 1c and a large amount of Ti element is detected on the electrode. However, the surface coating of Ti/TiO<sub>2</sub>-NW/SnO<sub>2</sub>-Sb electrode (Fig. 8b) is substantially unchanged compared to Fig. 1d and no Ti element is detected. Lim *et al.*<sup>46</sup> have proved that when the element content of Sb is between 5% and 10%, there is little difference in the effect on the electrode stability. Here, the main

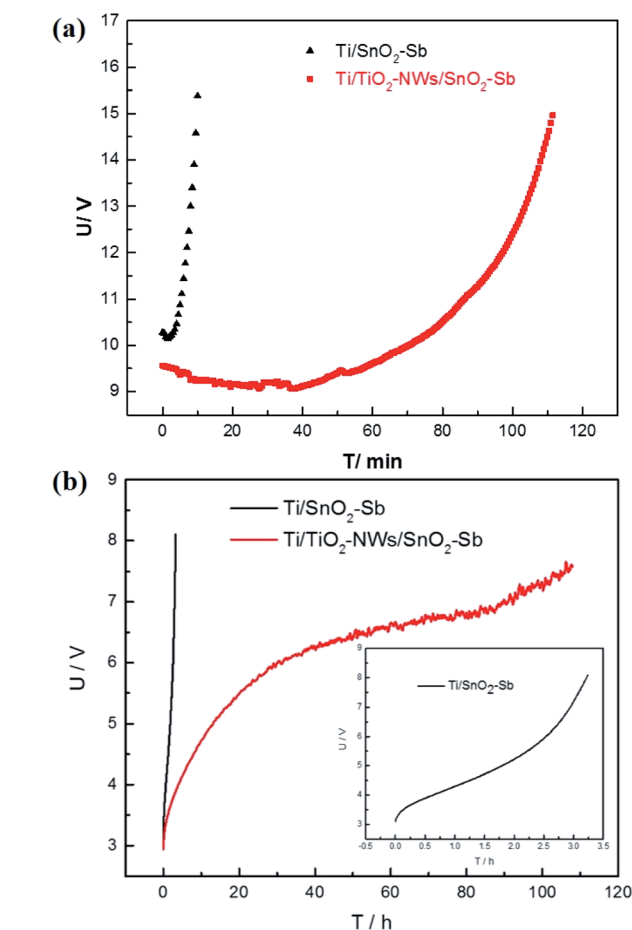


Fig. 7 (a) Accelerated service life of Ti/SnO<sub>2</sub>-Sb and Ti/TiO<sub>2</sub>-NW/SnO<sub>2</sub>-Sb electrodes in 0.5 M H<sub>2</sub>SO<sub>4</sub> with a current density of 1 A cm<sup>-2</sup>; (b) accelerated service life of Ti/SnO<sub>2</sub>-Sb and Ti/TiO<sub>2</sub>-NW/SnO<sub>2</sub>-Sb electrodes in 0.5 M H<sub>2</sub>SO<sub>4</sub> with a current density of 250 mA cm<sup>-2</sup>.

cause of electrode deactivation is the formation of a non-conductive layer of TiO<sub>2</sub>, which hinders the transfer of electrons. As shown in Fig. 8c,  $R_{\text{ct}}$  of the Ti/SnO<sub>2</sub>-Sb and Ti/TiO<sub>2</sub>-NW/SnO<sub>2</sub>-Sb electrode is 22 340 Ω and 258.4 Ω, respectively. Compared with Fig. 4, it means that the charge transfer resistance of Ti/SnO<sub>2</sub>-Sb electrode is nearly 250 times higher than that before the accelerated life test. However, the charge transfer resistance of the Ti/TiO<sub>2</sub>-NW/SnO<sub>2</sub>-Sb electrode is only increased by 14 times after the accelerated life test, which is still at a lower level. Because of the three-dimensional TiO<sub>2</sub>-NW, the resulting SnO<sub>2</sub>-Sb layer is dense and compact, which could insulate the Ti substrate from the corrosive acidic solution. As a result, the chance for forming a new non-conductive layer of

Table 3 The voltammetric charges and electrochemical porosity of different electrodes

Electrodes	$q_{\text{total}}/(\text{C cm}^{-2})$	$q_{\text{out}}/(\text{C cm}^{-2})$	$q_{\text{in}}/(\text{C cm}^{-2})$	$r$
Ti/SnO <sub>2</sub> -Sb	0.0118	0.0077	0.0041	0.347
Ti/TiO <sub>2</sub> -NW/SnO <sub>2</sub> -Sb	0.0192	0.0095	0.0097	0.505





Table 4 Accelerated life data of some previous works and this work

Electrodes	Test condition	Accelerated life	Accelerated life when current density converted to 100 mA cm <sup>-2</sup>	Ref.
Ti/TiO <sub>2</sub> -NW/SnO <sub>2</sub> -Sb	1 A cm <sup>-2</sup> , 0.5 M H <sub>2</sub> SO <sub>4</sub>	111.5 min	185.8 h	This work
	250 mA cm <sup>-2</sup> , 0.5 M H <sub>2</sub> SO <sub>4</sub>	108 h	675 h	
Ti/Ce-Mn/SnO <sub>2</sub> -Sb-La	1 A cm <sup>-2</sup> , 1 M H <sub>2</sub> SO <sub>4</sub>	85.2 min	142 h	41
Ti/Cu-NRs/SnO <sub>2</sub> -Sb	1 A cm <sup>-2</sup> , 0.5 M H <sub>2</sub> SO <sub>4</sub>	12 min	20 h	25
Ti/TiO <sub>2</sub> -NTs/SnO <sub>2</sub> -Sb	200 mA cm <sup>-2</sup> , 1 M H <sub>2</sub> SO <sub>4</sub>	31 h	124 h	42
Ti/TiO <sub>2</sub> H <sub>y</sub> /SnO <sub>2</sub> -Sb	200 mA cm <sup>-2</sup> , 0.5 M H <sub>2</sub> SO <sub>4</sub>	32 h	128 h	30
Ti/Pt/SnO <sub>2</sub> -Sb	100 mA cm <sup>-2</sup> , 1 M H <sub>2</sub> SO <sub>4</sub>	210 h	210 h	43
Ti/Sn-Sb/SnO <sub>2</sub> -F-Sb	100 mA cm <sup>-2</sup> , 0.5 M H <sub>2</sub> SO <sub>4</sub>	103.1 h	103.1 h	44
Ti/SnO <sub>2</sub> -Sb/SnO <sub>2</sub> -Sb	200 mA cm <sup>-2</sup> , 0.5 M H <sub>2</sub> SO <sub>4</sub>	10.7 h	42.8 h	45

TiO<sub>2</sub> on the Ti substrate becomes smaller and thus the service lifetime of the electrode is improved. As a comparison, the oxidation of the Ti substrate into TiO<sub>2</sub> in the Ti/SnO<sub>2</sub>-Sb

electrode is much easier and faster, because the Ti substrate is exposed in the corrosive acidic solution directly.

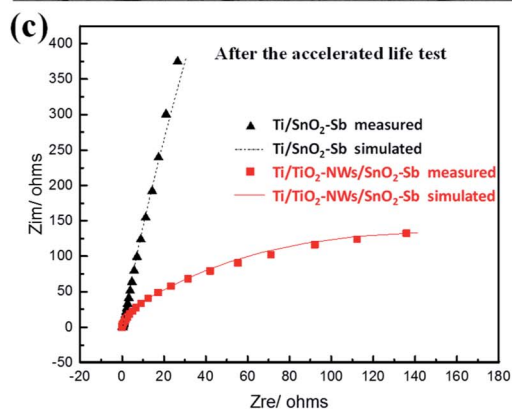
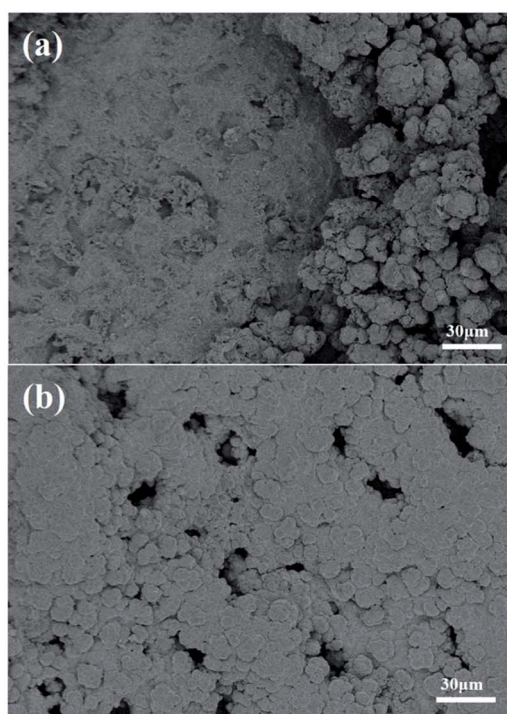


Fig. 8 (a) SEM image of Ti/SnO<sub>2</sub>-Sb electrode and (b) SEM image of Ti/TiO<sub>2</sub>-NW/SnO<sub>2</sub>-Sb electrode after the accelerated service life test at the current density of 1 A cm<sup>-2</sup>; (c) electrochemical impedance spectroscopies of Ti/SnO<sub>2</sub>-Sb and Ti/TiO<sub>2</sub>-NW/SnO<sub>2</sub>-Sb electrodes in 0.5 mol L<sup>-1</sup> H<sub>2</sub>SO<sub>4</sub> solution after the accelerated life test.

### 3.4. Electrochemical degradation of AR 73

In order to detect the electrocatalytic activity, two kinds of electrodes were used to degrade AR 73. Fig. 9a shows the evolution of AR 73 concentration as a function of time, and it can be found that the degradation of AR 73 by Ti/TiO<sub>2</sub>-NW/SnO<sub>2</sub>-Sb electrode can reach 98.6% after 5 h, while Ti/SnO<sub>2</sub>-Sb electrode is 89.1%. Meanwhile, the electrochemical degradation of AR 73 meets the pseudo first-order kinetics criterion.

$$\ln \frac{C_0}{C_t} = kt \quad (5)$$

where  $C_0$  is the initial concentration of AR 73,  $C_t$  is the concentration of AR 73 at given time  $t$  and  $k$  is the kinetic rate constant.<sup>47</sup> As shown in Fig. 9b, the kinetic rate constant of Ti/TiO<sub>2</sub>-NW/SnO<sub>2</sub>-Sb electrode is 0.749 h<sup>-1</sup>, which is 1.66 times that of the Ti/SnO<sub>2</sub>-Sb electrode (0.452 h<sup>-1</sup>). Apparently, the degradation rate of Ti/TiO<sub>2</sub>-NW/SnO<sub>2</sub>-Sb electrode was faster than that of the Ti/SnO<sub>2</sub>-Sb electrode at any time. From Table 1, the Sb content of the Ti/TiO<sub>2</sub>-NW/SnO<sub>2</sub>-Sb electrode is more than that of the Ti/SnO<sub>2</sub>-Sb electrode, which affects the generation of the  $\cdot\text{OH}$  of the Ti/TiO<sub>2</sub>-NW/SnO<sub>2</sub>-Sb electrode to some extent.<sup>48</sup> However, the degradation of AR 73 by Ti/TiO<sub>2</sub>-NW/SnO<sub>2</sub>-Sb electrode can reach 98.6% after 5 h, more than that of Ti/SnO<sub>2</sub>-Sb electrode's (89.1%). As a result, the content of Sb is not the main factor for the difference of the catalytic activity between Ti/SnO<sub>2</sub>-Sb electrode and Ti/TiO<sub>2</sub>-NW/SnO<sub>2</sub>-Sb electrode. The difference is mainly due to the surface morphology of the SnO<sub>2</sub>-Sb particles on the electrodes. The SnO<sub>2</sub>-Sb particles of Ti/TiO<sub>2</sub>-NW/SnO<sub>2</sub>-Sb electrode are smaller, which can provide a larger active area for degradation process. The result of CV also demonstrates the Ti/TiO<sub>2</sub>-NW/SnO<sub>2</sub>-Sb electrode has a larger electrochemical active specific surface area than Ti/SnO<sub>2</sub>-Sb electrode. With the deepening of the degradation progress, the cell voltage of the Ti/SnO<sub>2</sub>-Sb electrode rose rapidly (Fig. 9c). It is worth noting that the high cell voltage leads to an increase in the energy consumption of the electrode, and the high energy consumption will affect the practical application of electrode.

Fig. 9d shows the evolution of COD during the degradation process. The removal rate of Ti/TiO<sub>2</sub>-NW/SnO<sub>2</sub>-Sb electrode is



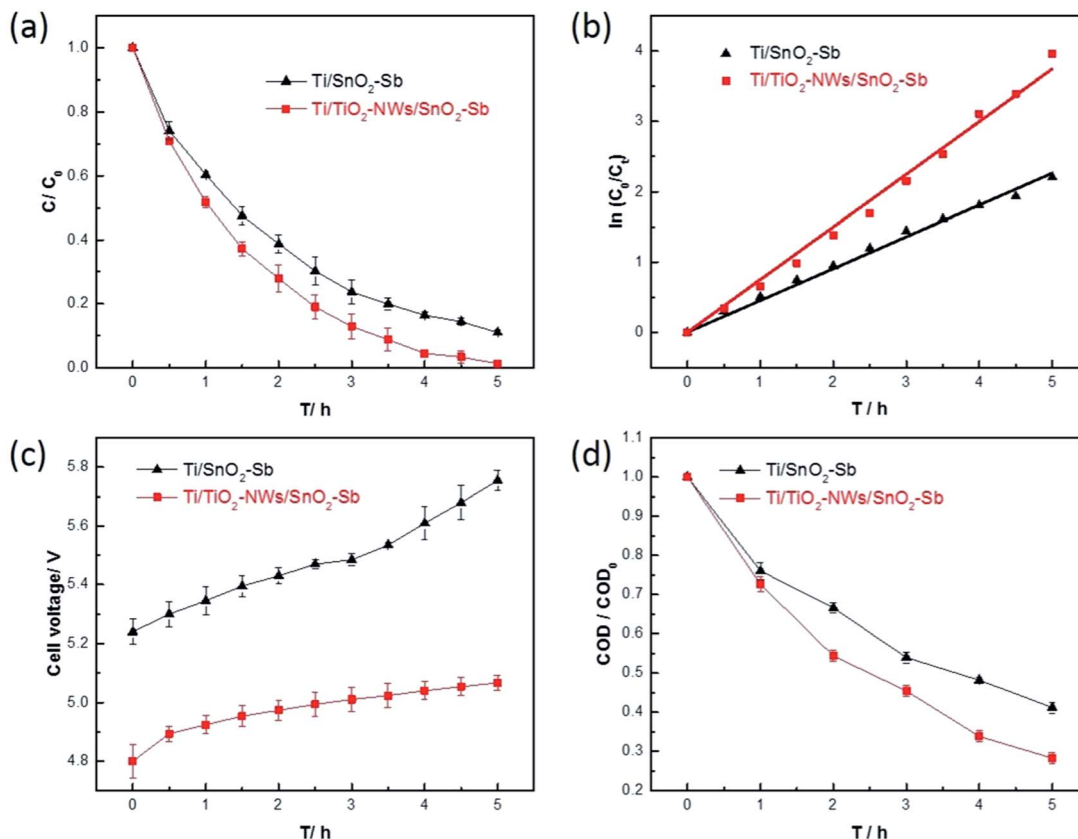


Fig. 9 (a) Evolution of the relative concentration of AR 73 during the degradation process; (b) kinetic rate constants of two electrodes; (c) evolution of the cell voltage; (d) evolution of the chemical oxygen demand (COD) during the degradation process ( $C_{AR\ 73} = 100\text{ mg L}^{-1}$ ,  $C_{Na_2SO_4} = 0.1\text{ mol L}^{-1}$ ,  $I = 20\text{ mA cm}^{-2}$ ).

71.8%, which is more than that of the  $Ti/SnO_2-Sb$  electrode (58.8%). This result further demonstrates that the  $Ti/TiO_2-NW/SnO_2-Sb$  electrode has a better electrocatalytic performance.

### 3.5. Energy consumption

In the industrial application of electrodes, besides the degradation ability and the service life, the economic rationality of the whole process also needs to be considered. Therefore, it is necessary to calculate the energy consumption of degradation process by

$$E = \frac{S \times i \times U}{V} t \quad (6)$$

where  $E$  is the energy consumption ( $\text{W h L}^{-1}$ ),  $S$  is the working area of the electrode ( $\text{cm}^2$ ),  $i$  is the current density ( $\text{mA cm}^{-2}$ ),  $U$  is the average cell voltage (V),  $V$  is the volume of AR 73 used in the degradation (mL) and  $t$  is the degradation time (h) which is calculated by eqn (5). In Fig. 10, the energy consumption of  $Ti/TiO_2-NW/SnO_2-Sb$  electrode is less than that of  $Ti/SnO_2-Sb$  electrode when the concentration of AR 73 reaches 80%, 60%, 40% and 20%, respectively. Especially when the concentration of AR 73 is 20%, the energy consumption of  $Ti/TiO_2-NW/SnO_2-Sb$  electrode is  $42.76\text{ W h L}^{-1}$ , which is 45.2% lower than that of  $Ti/SnO_2-Sb$  electrode ( $78.01\text{ W h L}^{-1}$ ). It can be seen from eqn (6) that the  $S$ ,  $i$ , and  $V$  values are equal under the same

degradation conditions. The average cell voltage of  $Ti/TiO_2-NW/SnO_2-Sb$  electrode (4.97 V) is lower than that of  $Ti/SnO_2-Sb$  electrode (5.48 V). Besides, the time required for the  $Ti/TiO_2-NW/SnO_2-Sb$  electrode is also shorter when degrading to the same concentration. Therefore, it is because of the low energy

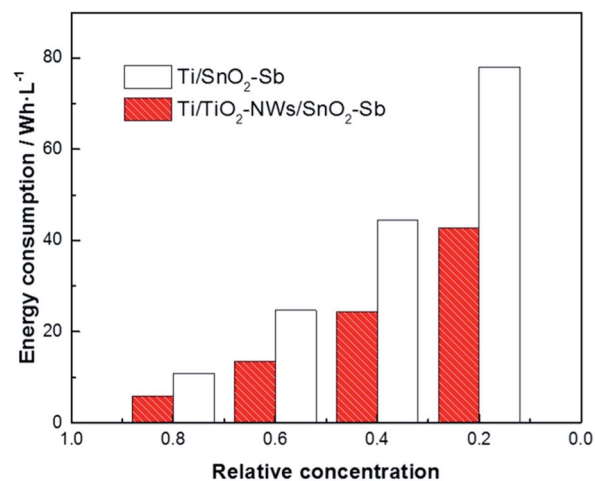


Fig. 10 Comparison of the energy consumption between  $Ti/SnO_2-Sb$  and  $Ti/TiO_2-NW/SnO_2-Sb$  electrodes in degradation process.





consumption that the Ti/TiO<sub>2</sub>-NW/SnO<sub>2</sub>-Sb electrode is more suitable for industrial applications.

## 4. Conclusions

In this paper, the Ti/TiO<sub>2</sub>-NW/SnO<sub>2</sub>-Sb electrode was fabricated by pulse electrodeposition of SnO<sub>2</sub>-Sb catalyst layer onto Ti substrate with TiO<sub>2</sub> network structure to enhance its service life. Compared to the traditional Ti/SnO<sub>2</sub>-Sb electrode without TiO<sub>2</sub>-NW, this novel electrode has a high oxygen evolution potential, a low charge transfer resistance and a larger electrochemical active surface area. More importantly, the introduction of the TiO<sub>2</sub> network structure prolongs the accelerated service life of the electrode to 111.5 min under 1 A cm<sup>-2</sup> current density, which is 11.15 times of that for the Ti/SnO<sub>2</sub>-Sb electrode. During a 5 hours' test, the AR 73 and COD removals can reach 98.6% and 71.8%, respectively, which are higher than those of Ti/SnO<sub>2</sub>-Sb electrode (89.1% and 58.8%). The energy consumption of the Ti/TiO<sub>2</sub>-NW/SnO<sub>2</sub>-Sb electrode is also lower than that of the Ti/SnO<sub>2</sub>-Sb electrode. In summary, this study highlights the long service life and excellent electrochemical activity of the Ti/TiO<sub>2</sub>-NW/SnO<sub>2</sub>-Sb electrode, and provides a stable and energy-efficient strategy for the degradation of dye wastewater.

## Conflicts of interest

There are no conflicts to declare.

## Acknowledgements

Our research was supported by the National Natural Science Foundation of China (Grand No. 11705126 and 21276177).

## References

- 1 E. Brillas and C. A. Martínez-Huitle, *Appl. Catal., B*, 2015, **166–167**, 603–643.
- 2 R. W. Gullick, M. W. Lechevallier and T. S. Barhorst, *J. - Am. Water Works Assoc.*, 2001, **93**, 66–77.
- 3 Y. Xu, R. Lebrun, P. Gallo and P. Blond, *Sep. Sci. Technol.*, 1999, **34**, 2501–2519.
- 4 S. S. Wong, T. T. Teng, A. L. Ahmad, A. Zuhairi and G. Najafpour, *J. Hazard. Mater.*, 2006, **135**, 378–388.
- 5 S. Vasudevan and M. A. Oturan, *Environ. Chem. Lett.*, 2014, **12**, 97–108.
- 6 F. Nabizadeh Chianeh and J. Basiri Parsa, *Chem. Eng. Res. Des.*, 2014, **92**, 2740–2748.
- 7 M. Panizza and G. Cerisola, *Chem. Rev.*, 2009, **109**, 6541–6569.
- 8 Y. J. Feng and X. Y. Li, *Water Res.*, 2003, **37**, 2399–2407.
- 9 X. Chen and G. Chen, *Electrochim. Acta*, 2005, **50**, 4155–4159.
- 10 G. Li, S. Zhou, Z. Shi, X. Meng, L. Li and B. Liu, *Environ. Sci. Technol.*, 2019, **26**, 17740–17750.
- 11 H. Li, X. Zhu, Y. Jiang and J. Ni, *Chemosphere*, 2010, **80**, 845–851.
- 12 J. Wu, H. Xu and W. Yan, *RSC Adv.*, 2015, **5**, 19284–19293.
- 13 B. Wang, W. Kong and H. Ma, *J. Hazard. Mater.*, 2007, **146**, 295–301.
- 14 S. Y. Yang, D. Kim and H. Park, *Environ. Sci. Technol.*, 2014, **48**, 2877–2884.
- 15 Y. Feng, Y. Cui, B. Logan and Z. Liu, *Chemosphere*, 2008, **70**, 1629–1636.
- 16 T. Duan, Y. Chen, Q. Wen and Y. Duan, *RSC Adv.*, 2015, **5**, 19601–19612.
- 17 L. Xu, Y. Wang, Q. Xu and H. Duan, *J. Electrochem. Soc.*, 2019, **166**, E69–E76.
- 18 Q. Zhuo, S. Deng, B. Yang, J. Huang and G. Yu, *Environ. Sci. Technol.*, 2011, **45**, 2973–2979.
- 19 X. Lei, L. Li, Y. Chen and Y. Hu, *Environ. Sci. Pollut. Res.*, 2018, **25**, 11683–11693.
- 20 L. Xu and Y. Lian, *J. Electrochem. Soc.*, 2016, **163**, H1144–H1150.
- 21 L. Wang, Y. Wang, S. Wang, H. Zhang, Y. Kang and W. Huang, *Sens. Actuators, B*, 2013, **188**, 85–93.
- 22 L. K. Xu and J. D. Scantlebury, *Corros. Sci.*, 2003, **45**, 2729–2740.
- 23 F. Vicent, E. Morallo N, C. Quijada, J. L. Va Zquez, A. Aldaz and F. Cases, *J. Appl. Electrochem.*, 1998, **28**, 607–612.
- 24 Y. Chen, L. Hong, H. Xue, W. Han, L. Wang, X. Sun and J. Li, *J. Electroanal. Chem.*, 2010, **648**, 119–127.
- 25 W. Xu, L. Xu and M. Li, *Electrochim. Acta*, 2015, **166**, 64–72.
- 26 A. Xu, X. Dai, K. Wei, W. Han, J. Li, X. Sun, J. Shen and L. Wang, *RSC Adv.*, 2017, **7**, 37806–37814.
- 27 T. Duan, L. Ma, Y. Chen, X. Ma, J. Hou, C. Lin and M. Sun, *J. Solid State Electrochem.*, 2018, **22**, 1871–1879.
- 28 P. Li, G. Zhao, X. Cui, Y. Zhang and Y. Tang, *J. Phys. Chem. C*, 2009, **113**, 2375–2383.
- 29 X. Li, Z. Zhu, G. P. Nayaka, J. Duan, D. Wang, P. Dong, L. Huang, J. Zhao, S. Sun, X. Yu and Y. Zhang, *J. Alloys Compd.*, 2018, **752**, 68–75.
- 30 X. Li, D. Shao, H. Xu, W. Lv and W. Yan, *Chem. Eng. J.*, 2016, **285**, 1–10.
- 31 F. Montilla, E. Morallón, A. De Battisti and J. L. Vázquez, *J. Phys. Chem. B*, 2004, **108**, 5036–5043.
- 32 X. Cui, G. Zhao, Y. Lei, H. Li, P. Li and M. Liu, *Mater. Chem. Phys.*, 2009, **113**, 314–321.
- 33 F. Montilla, E. Morallón, A. De Battisti, A. Benedetti, H. Yamashita and J. L. Vázquez, *J. Phys. Chem. B*, 2004, **108**, 5044–5050.
- 34 F. Oliveira, M. Osugi, F. Paschoal, D. Profeti, P. Olivi and M. Zanoni, *J. Appl. Electrochem.*, 2007, **37**, 583–592.
- 35 G. Zhao, X. Cui, M. Liu, P. Li, Y. Zhang, T. Cao, H. Li, Y. Lei, L. Liu and D. Li, *Environ. Sci. Technol.*, 2009, **43**, 1480–1486.
- 36 O. Simond, V. Schaller and C. Comninellis, *Electrochim. Acta*, 1997, **42**, 2009–2012.
- 37 L. Bao, J. Zang and X. Li, *Nano Lett.*, 2011, **11**, 1215–1220.
- 38 R. Berenguer, C. Quijada and E. Morallón, *Electrochim. Acta*, 2009, **54**, 5230–5238.
- 39 Y. Chang, L. Deng, X. Meng, W. Zhang, C. Wang, Y. Wang, S. Zhao, L. Lin and J. C. Crittenden, *Environ. Sci. Technol.*, 2018, **52**, 5940–5948.
- 40 F. Hine, M. Yasuda, T. Noda, T. Yoshida and J. Okuda, *J. Electrochem. Soc.*, 1979, **126**, 1439–1445.



- 41 Q. Bi, W. Guan, Y. Gao, Y. Cui, S. Ma and J. Xue, *Electrochim. Acta*, 2019, **306**, 667–679.
- 42 R. A. Subba and V. T. Venkatarangaiah, *Environ. Sci. Pollut. Res.*, 2018, **25**, 11480–11492.
- 43 C. Shao, J. Yu, X. Li, X. Wang and K. Zhu, *J. Electroanal. Chem.*, 2017, **804**, 140–147.
- 44 B. Yang, J. Wang, C. Jiang, J. Li, G. Yu, S. Deng, S. Lu, P. Zhang, C. Zhu and Q. Zhuo, *Chem. Eng. J.*, 2017, **316**, 296–304.
- 45 D. Shao, X. Li, H. Xu and W. Yan, *RSC Adv.*, 2014, **4**, 21230–21237.
- 46 D. Lim, Y. Kim, D. Nam, S. Hwang, S. E. Shim and S. Baeck, *J. Cleaner Prod.*, 2018, **197**, 1268–1274.
- 47 Q. Wang, T. Jin, Z. Hu, M. Zhou and L. Zhou, *Sep. Purif. Technol.*, 2013, **102**, 180–186.
- 48 Y. Cui and Y. Feng, *J. Mater. Sci.*, 2005, **40**, 4695–4697.

